Large-Scale Heliospheric Structure during Solar-Minimum Conditions using a 3D Time-Dependent Reconstruction Solar-Wind Model and STELab IPS Observations

M.M. Bisi*, B.V. Jackson*, P.P. Hick*,†, J.M. Clover*, S. Hamilton*, M. Tokumaru** and K. Fujiki**

*Center for Astrophysics and Space Sciences, University of California, San Diego, 9500 Gilman Drive #0424, La Jolla, 92093-0424 CA USA
†San Diego Supercomputer Center, University of California, San Diego, 9500 Gilman Drive #0505, La Jolla, 92093-0505 CA USA
**Solar-Terrestrial Environment Laboratory (STELab), Nagoya University, Furo-cho, Chikusa-ku, Nagoya 464-8601, Japan

Abstract. Interplanetary scintillation (IPS) observations provide information about a large portion of the inner heliosphere. We have used Solar-Terrestrial Environment Laboratory (STELab) IPS velocity and *g*-level observations with our three-dimensional (3D) reconstruction model to determine velocities and densities of the inner heliosphere in three dimensions. We present these observations using synoptic maps generated from our time-dependent model that can measure changes with durations of less than one day. These synopses show large-scale stable solar-wind structure during solar-minimum conditions in relation to transients that are present during this period. These are also available as differences relative to the background. Here, we concentrate primarily on data covering the 2007-2009 International Heliophysical Year (IHY).

Keywords: Solar Wind, Solar Minimum Cycle, Interplanetary Coronal Mass Ejections (ICMEs), Three-Dimensional (3D) Heliospheric Velocity and Density Reconstructions
PACS: 96.50.-e, 96.60.ph, 96.50.Wx

INTRODUCTION

Interplanetary Scintillation (IPS) is the rapid variation in radio signal from a compact distant natural source produced by turbulence and variations in the solar wind density, e.g., [1]. Measurements of IPS allow the solar wind velocity (and an inferred value of density) to be observed over a large range of heliographic latitudes and at distances from the Sun currently inaccessible by spacecraft – no other observing method has the unique capabilities of IPS.

Two-antenna observations of IPS are where simultaneous recordings are made of the same radio source by widely-separated antennas; this allows the solar wind velocity to be measured to a high degree of accuracy (with the underlying assumption of radial outflow). Density values for the solar wind can be inferred from the "scintillation level" (*g*-level) of IPS observations.

Data from IPS observations using the Solar-Terrestrial Environment Laboratory (STELab) arrays, Nagoya University, Japan [2], are routinely used for the time-dependent three-dimensional (3D) tomographic reconstructions (as in this paper). Our real-time STELab IPS solar wind forecasts (April/May through November/December of each year) are available at: `http://ips.ucsd.edu/`.

Figure 1 (taken from [3]) shows the mapping of portions of the lines of sight of the IPS observations down to the solar surface throughout Carrington rotation (CR) 2068 (the Whole Heliosphere Interval – WHI) in Carrington latitude (vertical axis) and longitude (horizontal axis). This is an example of how the IPS lines of sight (or portions of) map down onto the "source surface" before being propagated out into the heliosphere to make up the 3D structure of the inner heliosphere out to 3 AU using our heliospheric Computer-Assisted Tomography (C.A.T.) analysis.

The 3D reconstructions with our time-dependent model have a one-day cadence and 20° × 20° digital resolution for current STELab IPS data. These resolutions are predicated by the numbers of lines of sight available for the reconstructions. For details on the 3D reconstructions see [4, 5] and references therein.

In this paper, we describe our 3D reconstructions for the International Heliophysical Year (IHY – 2007-2009) STELab IPS observations, provide a preliminary study of an interplanetary coronal mass ejection (ICME) seen using the same technique (2008/06/02-2008/06/06), and then we conclude and discuss some future prospects.

CP1216, *Twelfth International Solar Wind Conference,*
edited by M. Maksimovic, K. Issautier, N. Meyer-Vernet, M. Moncuquet, and F. Pantellini

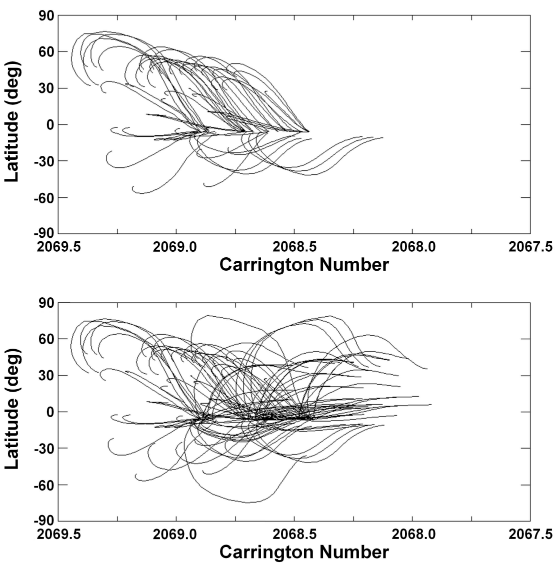

FIGURE 1. The STELab IPS lines of sight used by the 3D tomography from scintillation level (top) and velocity (bottom) observations mapped back to 15 $R_\odot$ which is the source surface (lower boundary) in the 3D tomography. As can be seen, the velocity coverage is far greater over the two Carrington rotations used for the tomography (CR2067.50 to CR2069.50) than that of *g*-level coverage; a difference in the number of velocity versus *g*-level observations can occur due to outages at one or more of the STELab IPS arrays used to provide data. Figure taken from [3].

CURRENT SOLAR MINIMUM CONDITIONS

For each rotation where IPS data were available from STELab for the IHY, we performed our time-dependent 3D reconstructions (CR2056-CR2063, CR2068-CR2077, and with preliminary data for CR2083, inclusive) for both velocity and density. Each CR was separately averaged in velocity and density to provide a rotation-averaged synoptic map at the model source surface of 15$R_\odot$, and at the near-Earth distance of 1 AU. These were used to study velocity and density structure of the solar wind during this time from differences between the averaged Carrington-rotation synopses and the individual daily plots.

Figure 2 shows rotation-averaged Carrington plots from the 3D reconstructions at the model source surface for CR2058 (left), CR2074 (middle), and CR2083 (right). The top plots display the IPS velocity distribution, and the bottom plots display the density distribution. As can be seen from the overall structure early in the IHY period (CR2058), the Sun was beginning to show signs of what we would typically expect for solar minimum conditions. However, from the two later rotations (CR2074 and CR2083), the picture is clearly not a simple dipolar velocity distribution (although in CR2083, the distribution starts to get more towards dipolar again) or a simple higher-density streamer belt as compared with the mid-latitude to polar regions. This unusual structure is also consistent with findings by [6] who also used these IPS data in their analyses.

From a time-dependent reconstructed synoptic map on a particular day, you can subtract these rotation-averaged synoptic maps in order to look for velocity and density depletions and enhancements relative to the rotation mean. These can aid in finding transients (and perhaps co-rotating features) in the reconstructions and enable us to compare positions and timing with those from coronagraph observations as is done in the next section.

PRELIMINARY EXAMPLE OF AN ICME

Here, we use our rotation-averaged synoptic maps and subtract these from each of the daily-reconstructed synoptic maps from the time-dependent tomography in order to look for transient features as mentioned in the previous section.

A coronal mass ejection (CME) can be seen in the SOlar and Heliospheric Observatory – Large Angle and Spectroscopic COronagraph (SOHO|LASCO) C2 and C3 instruments' [7, 8] difference images and the C2/Extreme-ultraviolet Imaging Telescope (EIT – also aboard SOHO) [9] composite image first clearly seen in C2 at 04:55 UT on 2008/06/02 during CR2070 going to the East of the Sun around the ecliptic plane as shown in the LASCO images: Figures 3 and 4.

The 3D tomography shows a likely slow velocity for the CME which is approximately consistent with the LASCO height-time plot (also shown here as Figure 5). The Carrington plots are displayed as difference images from the tomography (Figure 6) between the rotation-averaged synopses and the individual daily maps of what is reconstructed at 1 AU on 2008/06/06 at the time the CME is extrapolated to reach an approximate distance from the Sun of 1 AU for both velocity (top) and density (bottom). These SOHO images are taken from the Coordinated Data Analysis Workshops (CDAW) catalog:
`http://cdaw.gsfc.nasa.gov/CME_list/`
and are courtesy of the SOHO|LASCO and SOHO|EIT Consortia.

Preliminary analyses suggest that the enhancement in density in the differenced-density Carrington plot is correctly positioned (grossly between 15° and 60° Carrington Longitude) for the CME to be arriving at 1 AU; as well as the diminished velocity since this was a slow-moving CME below that of the average velocity for the rotation around this region (clear/white circles). Figure 7 displays the density reconstruction in the ecliptic which

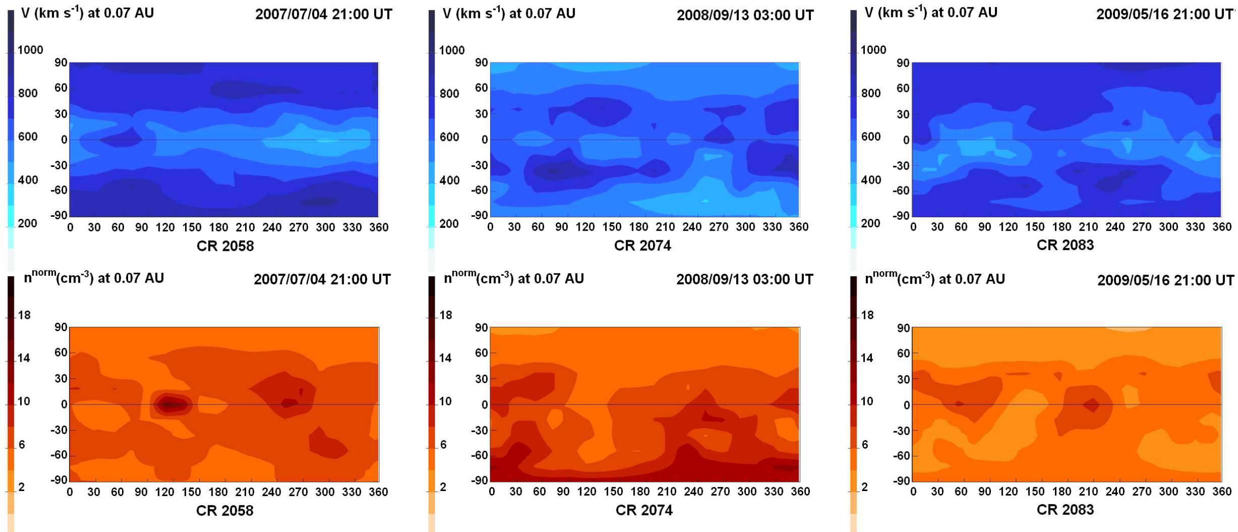

FIGURE 2. Carrington-rotation-averaged 3D-reconstructed velocity (top) and density (bottom) results at the model source surface displayed as synoptic maps for three Carrington rotations: CR2058, CR2074, and CR2083 (from left to right). Further details can be found in the text.

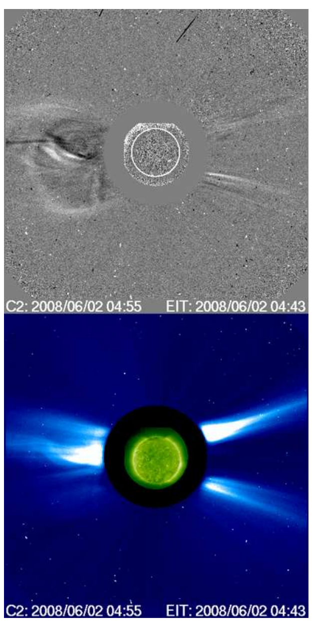

FIGURE 3. The SOHO C2 and EIT Composite images for differenced (top) and direct (bottom) observations of the 2008/06/02 CME.

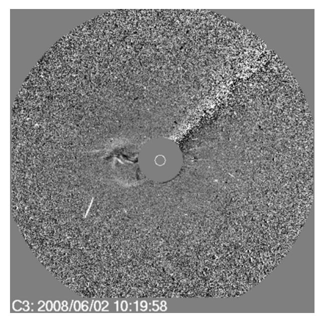

FIGURE 4. The SOHO C3 differenced image of the same CME as in Figure 3 showing it's extent early on in this instrument's field of view.

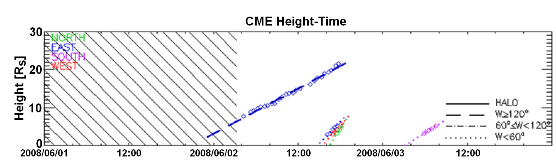

FIGURE 5. The height-time (elongation-time) plot of the 2008/06/02 CME taken from the CDAW CME list. Unfortunately, LASCO was down until early on 2008/06/02 and thus was only able to measure the CME from a height of around 8 $R_{\odot}$. Further details can be found in the text.

also shows the ICME is directed toward the Solar TErrestrial RElations Observatory (STEREO) [10, 11] behind (STEREO-B) spacecraft (further investigation will be the subject of a future paper).

These findings are consistent with those of the "source-less" CME described by [12] according to A. Vourlidas [private communication, 2009].

SUMMARY AND FUTURE PROSPECTS

The 3D reconstructions displayed as source-surface rotation-averaged Carrington maps show the unusual solar wind velocity and density distribution during the

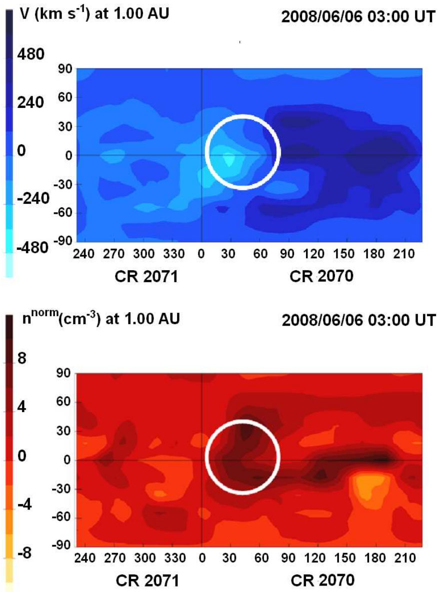

FIGURE 6. Differenced Carrington synoptic maps at 1 AU (at the time shown) of velocity (top) and density (bottom) from our 3D tomographic reconstructions. Positive values (darker regions) are enhancements to the mean, and negative values (lighter regions) are depletions/reductions from the mean. The area circled is the broad region at 1 AU where the ICME relating to the 2008/06/02 CME is seen. Further details can be found in the text.

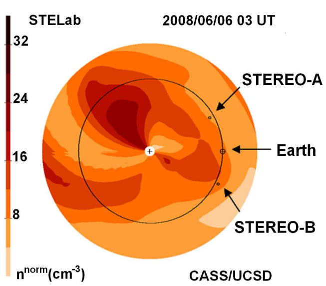

FIGURE 7. An ecliptic-cut extraction from the 3D tomographic reconstruction in density as looking down from the North on 2008/06/06 at 0300 UT. Displayed and marked are the positions of Earth and the two STEREO spacecraft; the ICME can be seen heading between the Earth and the STEREO-B spacecraft. Further details can again be found in the text.

present long and seemingly "unconventional" solar minimum. Preliminary use of differenced Carrington synoptic maps show ICME signatures traced back to the source surface which compare with SOHO|LASCO images and later the reconstructions show it is possibly directed toward one of the two STEREO spacecraft.

The future aim is to use this technique for a larger number of transient-type features and also to compare further with white-light imaging from the twin STEREO spacecraft and the Solar Mass Ejection Imager (SMEI), e.g., [13].

ACKNOWLEDGMENTS

We acknowledge and thank the NSF (grants ATM0331513, ATM0852246, and ATM0925023), NASA (grant NNX08AJ116), and AFOSR (grant FA9550-06-1-0107) for their funding. All SOHO images used in this article are taken from the Coordinated Data Analysis Workshops (CDAW) CME catalog which is generated and maintained at the CDAW Data Center by NASA and The Catholic University of America in cooperation with the Naval Research Laboratory. SOHO is a project of international cooperation between ESA and NASA.

REFERENCES

1. A. Hewish, P. F. Scott, and D. Wills, *Nature* **203**, 1214 (1964).
2. M. Kojima, and T. Kakinuma, *J. Geophys. Res.* **92**, 7269–7279 (1987).
3. M. M. Bisi, B. V. Jackson, A. Buffington, J. M. Clover, P. P. Hick, and M. Tokumaru, *Solar Phys.* **256**, 201–217 (2009).
4. B. V. Jackson, and P. P. Hick, *Astrophys. and Space Sci. Lib.* **314**, 355–386 (2005).
5. M. M. Bisi, B. V. Jackson, P. P. Hick, A. Buffington, D. Odstrcil, and J. M. Clover, *J. Geophys. Res.* **113**, A00A11 (2008).
6. M. Tokumaru, M. Kojima, K. Fujiki, and K. Hayashi, *Geophys. Res. Lett.* **36**, L091001 (2009).
7. V. Domingo, B. Fleck, and A. I. Poland, *Space Sci. Rev.* **72**, 81–84 (1995).
8. G. E. Brueckner, R. A. Howard, M. J. Koomen, C. M. Korendyke, D. J. Michels, J. D. Moses, D. G. Socker, K. P. Dere, P. L. Lamy, A. Llebaria, M. V. Bout, R. Schwenn, G. M. Simnett, D. K. Bedford, and C. J. Eyles, *Solar Phys.* **162**, 357–402 (1995).
9. J. P. Delaboudinière, G. E. Artzner, J. Brunaud, A. Gabriel, J. F. Hochedez, F. Millier, X. Y. Song, B. Au, K. P. Dere, R. A. Howard, R. Kreplin, D. J. Michels, J. D. Moses, J. M. Defise, C. Jamar, P. Rochus, J. P. Chauvineau, J. P. Marioge, R. C. Catura, J. R. Lemen, L. Shing, R. A. Stern, J. B. Gurman, W. M. eupert, A. Maucherat, F. Clette, P. Cugnon, and E. L. van Dessel, *Solar Phys.* **162**, 291–312 (1995).
10. M. L. Kaiser, *Adv. Space Res.* **36**, 1483–1488 (2005).
11. M. L. Kaiser, T. A. Kucera, J. M. Davila, O. C. St. Cyr, M. Guhathakurta, and E. Christian, *Space Sci. Rev.* **136**, 5–16 (2008).
12. E. Robbrecht, S. Patsourakos, and A. Vourlidas, *Astrophys. J.* **701**, 283–291 (2009).
13. C. J. Eyles, G. M. Simnett, M. P. Cooke, B. V. Jackson, A. Buffington, P. P. Hick, N. R. Waltham, J. M. King, P. A. Anderson, and P. E. Holladay, *Solar Phys.* **217**, 319–347 (2003).